Eur Biophys J (1999) 28: 591–599

ARTICLE

Dietrich Gradmann · Carl M. Boyd

Electrophysiology of the marine diatom *Coscinodiscus wailesii* IV: types of non-linear current-voltage-time relationships recorded with single saw-tooth voltage-clamp experiments

Received: 23 December 1998 / Revised version: 1 June 1999 / Accepted: 1 June 1999

Abstract Electrophysiological states of the marine diatom *Coscinodiscus wailesii* are known to change spontaneously in the temporal range of seconds. In order to assess the genuine current-voltage-time relationships of individual states in less than a second, voltage-clamp experiments have been carried out using single sweeps of saw-tooth shaped command voltages. This method is introduced with model calculations. Plotting the results in current-voltage coordinates provides convenient access to several electrophysiological entities, such as absence of drift (smoothly closed *IV* loops), membrane capacitance (by I jump at sign reversal of dV/dt), and ohmic conductances (in linear regions of the current-voltage relationship), as well as equilibrium voltage (internal intersection of capacitance-corrected, 8-shaped tracings) and coarse gating kinetics (rise or fall of capacitance-corrected I at sign reversal of dV/dt) of a voltage-sensitive ion conductance. From electrophysiological measurements with double-barreled glass-microelectrodes on *C. wailesii*, several distinct types of current-voltage loops are presented. Most of the data, including recordings from electrical excitation, can be interpreted as temporal relaxations of voltage-sensitive conductances for K^+ and Cl^-. A more detailed analysis of the effect of tetraethylammonium (TEA^+) shows that 10 and 20 mM TEA^+ inhibit the K^+ conductance in *C. wailesii* only by up to about 20% but predominantly via a K^+ outward rectifier.

D. Gradmann (✉)[1] · C.M. Boyd
Department of Oceanography,
Dalhousie University,
Halifax, N.S., Canada B3H 4J1

Present address:
[1]Abteilung Biophysik der Pflanze,
Albrecht-von-Haller-Institut für Pflanzenwissenschaften
der Georg-August-Universität,
Untere Karspüle 2,
D-37073 Göttingen, Germany
e-mail: dgradma@gwdg.de

Key words *Coscinodiscus wailesii* · Current-voltage relationships · K^+ currents · Marine diatoms · Ramp currents

Introduction

Step- and ramp-shaped time courses of the command voltage are widely used protocols in voltage-clamp studies of non-linear electrical properties of biomembranes. Step protocols are commonly used to investigate current-voltage relationships and their temporal changes. Step protocols have the disadvantage of protracted recording times, during which the membrane may change its electrical characteristics. Alternatively, ramp protocols are commonly employed, when the current-voltage characteristics are to be recorded within a short time. These recordings frequently suffer from applying only unidirectional ramps from one voltage V_1 to another voltage V_2 with a fixed slope, omitting complementary control recordings with reverse ramps (from V_2 to V_1) and with different ramp slopes. Although application of unidirectional ramps is still common (e.g. Frey et al. 1998), triangular ramps are used in some recent studies as well (e.g. Svirskis and Hounsgaard 1998).

The disadvantages of the step and of the ramp protocol can be overcome by using a single sweep of a saw-tooth shaped voltage cycle. In principle, any shape of voltage course, such as sine waves or triangular shapes with different slopes, could be used for this purpose. Here, we focus on a time course, with alternating positive and negative V/t slopes of the same amount.

This protocol provides immediate access to several electrophysiological entities, such as membrane capacitance (from I jump at sign reversal of dV/dt) and ohmic conductances (from linear regions of the current-voltage relationship), as well as equilibrium voltage (from internal intersection of the 8-shaped, capacitance-corrected tracings) and approximate gating kinetics of an ion

conductance with voltage-sensitive activity (from rise or fall of capacitance-corrected I at sign reversal of dV/dt).

It is known that the cells of *Coscinodiscus* change their electrophysiological state spontaneously and that such states may last for less than a minute (Gradmann and Boyd 1975; Boyd and Gradmann 1999a, b; Gradmann and Boyd 1999). Therefore, for investigation of such short electrophysiological states, methods must be used which allow recording of the current-voltage-time relationship of a particular state within a short time, and which allow the analysis of the data without compromising the goals of the study.

The two aims of this study are to present the methods for such fast recordings and to show examples of application of this method which reveal distinct electrophysiological characteristics of *Coscinodiscus*.

Materials and methods

The cells and electrophysiological setup have been described previously in detail (Boyd and Gradmann 1999a). Briefly, cylindrical cells of the marine diatom *Coscinodiscus wailesii* (strain 768 from North Eastern Culture Collection, Vancouver, B.C., Canada) have been used because of their large size (radius about 100 μm, altitude about 100 μm, in rare cases up to 200 μm) which reduces the relative artifact due to impalement of glass micropipettes. Voltage-clamp experiments have been carried out using a voltage-clamp circuit (Dagan 200 TEV) and double-barreled microelectrodes for voltage recording and for current injection. The medium surrounding a cell could be exchanged within a few seconds by directing a gentle jet of defined medium onto the cell under investigation.

Data acquisition and control of the voltage-clamp circuit were carried out via an AD/DA converter (Keithley System 500 KDAC). Personal computers have been used to run custom tailored software for AD/DA conversion and for data processing. The time courses of the transmembrane voltage, V (free running or under voltage-clamp control), and of the clamp current, I, were recorded in the computer. Simultaneously, the results have continuously been displayed with high temporal resolution on a digital oscilloscope, and recorded with low temporal resolution on a strip chart recorder for immediate inspection and for convenient scanning of the results.

Theory

The simple model shown in Fig. 1 serves to demonstrate the basic features of non-linear current-voltage-time relationships of a membrane, consisting of a membrane capacitance C_m (e.g. of 2 nF like in a cell of *C. wailesii*)

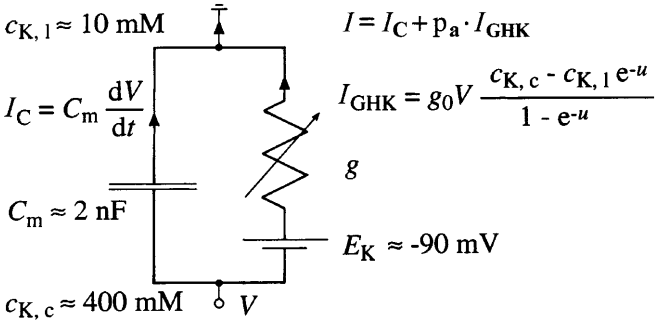

Fig. 1 Model system for a membrane with non-linear current-voltage-time relationships

and a pathway for electrodiffusion of K^+. The elements of this pathway (e.g. channels) can be either in an active (open) state a or in an inactive (closed) state i. When all elements are active, the current through this pathway can be written according to the constant-field current equation by Goldman, Hodgkin, and Katz (reviewed by Hodgkin 1951):

$$I_{GHK} = g_0 V_m \frac{c_{K,c} - c_{K,l} e^{-u}}{1 - e^{-u}} \quad (1)$$

where g_0 is the conductance when both the K^+ concentrations on the cytoplasmic side ($c_{K,c}$) and on the luminal side ($c_{K,l}$) are at a reference value (e.g. 1 mM), and u is the normalized membrane voltage; $u = FV_m/RT$ with F, R, and T having the usual thermodynamic meanings. In our assumed case of activation by negative voltages via a symmetric Eyring barrier, the transitions between a and i occur with the rate constants k_a for activation and k_i for inactivation:

$$k_a = k_a^0 e^{-u/2} \quad (2a)$$

$$k_i = k_i^0 e^{u/2} \quad (2b)$$

where the superscript 0 marks the rate constant at zero voltage. For our model system we choose $k_a^0 = 1\ s^{-1}$ and $k_i^0 = 10\ s^{-1}$. If p_a and p_i are the probabilities of the pathway to be active and inactive, respectively, these probabilities follow the differential equations

$$\frac{dp_a}{dt} = -k_i p_a + k_a p_i \quad (3a)$$

$$\frac{dp_i}{dt} = k_i p_a - k_a p_i \quad (3b)$$

The total current through the membrane is then

$$I = C_m dV/dt + p_a I_{GHK} \quad (4)$$

Figure 2 shows the behavior of the model system in Fig. 1 under voltage clamp with a saw-tooth shaped command voltage. The suggested voltage protocol starts with a short period at a steady state control voltage, V_0, which may be close to the resting or equilibrium voltage of the system. Then the voltage moves with a constant slope to a minimum voltage, V_1, where the slope changes

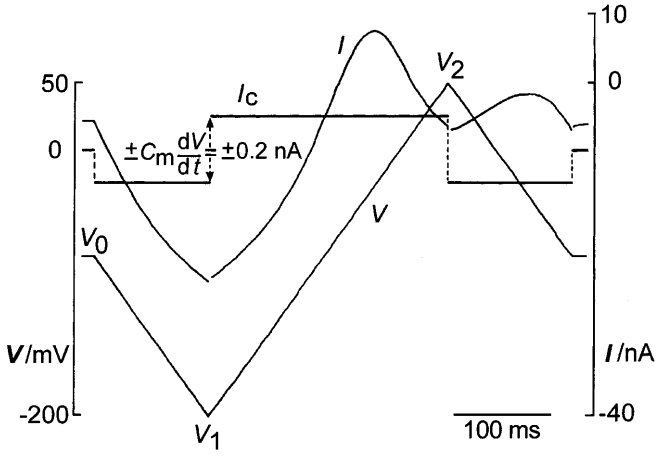

Fig. 2 Calculated time courses of total membrane current, I, and capacitive current, I_c (C_m = 2 nF) of the model system (Fig. 1) at 10 mM $c_{K,i}$ and 400 mM $c_{K,c}$, for an individual saw-tooth cycle of the command voltage (= V_m) over a voltage range from V_1 = −200 mV to V_2 = +50 mV, consisting of three linear slopes with dV/dt = ±0.1 V s^{-1} between control periods (here 200 ms) of V_m = V_0 = const. = −80 mV

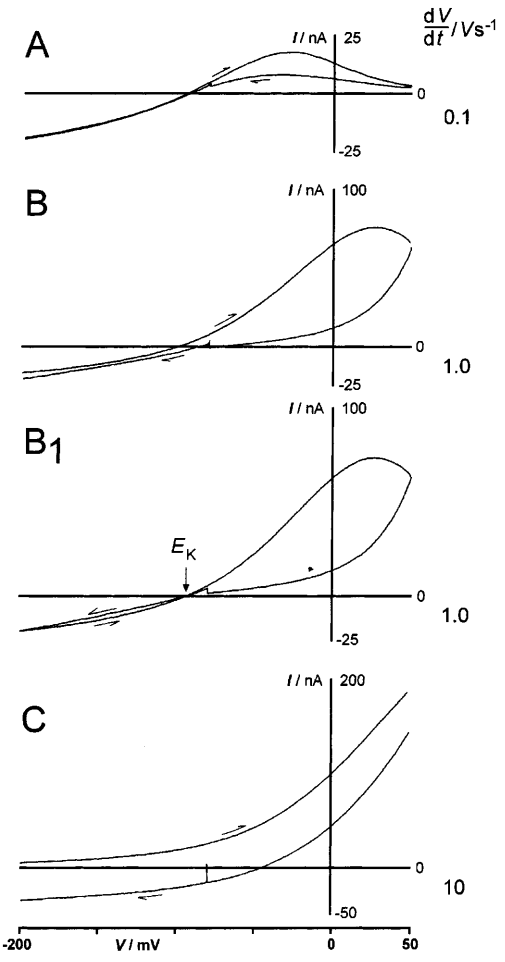

Fig. 3 Calculated current-voltage loops of model system (Fig. 1) upon single saw-tooth command voltages as in Fig. 2 with different slopes dV/dt: **A** dV/dt = 0.1 V s^{-1} (same as in Fig. 2); **B** dV/dt = 1.0 V s^{-1}; **B$_1$** as **B** but with C_m = 0; **C** dV/dt = 10 V s^{-1}

its sign and the voltage moves to a maximum voltage, V_2. Here, the slope reverses again, and the voltage moves back to V_0, where it is kept constant for another short time interval. The time course of the clamp current I through the model system upon such a saw-tooth shaped command voltage with a slope of 0.1 V s^{-1} is shown in Fig. 2 as well. This $I(t)$ tracing exhibits non-linear features which contain all the properties of the model system. In such diagrams, the capacitive current $I_C = C_m\, dV/dt$ can readily be identified. Although it can hardly be seen in the $I(t)$ tracing in Fig. 2, its discontinuous change by $2|dV/dt|C_m$ = 0.4 nA becomes obvious when the slope changes its sign at V_1 and at V_2. I_C is also plotted in Fig. 2 in an expanded I scale.

The $V(t)$ and $I(t)$ data from Fig. 2 are converted to the current-voltage diagram, $I(V)$, in Fig. 3A. Knowing the general shape of the saw-tooth voltage-protocol and $|dV/dt|$ (= 0.1 V s^{-1} in this case), Fig. 3A provides in principle the complete information from Fig. 2 which can be used to identify the four free parameters (C_m, g_0, k_a^0, and k_i^0) of the model system in Fig. 1. In contrast to Fig. 3B and C, the particular $|dV/dt|$ in Fig. 3A was too small to reveal the first parameter, C_m, by the capacitive currents. The second parameter $g_0 = g(V \ll 0)/c_{K,i}$, can be determined by $g(V \ll 0)$, i.e. the asymptotic straight I/V line (not drawn) through the origin which is approached by the left portion of the curve. The remaining parameters k_a^0 and k_i^0 can be determined by the right part of the graph, e.g. by the two currents at zero voltage, $I_{+,V=0}$ and $I_{-,V=0}$ for rising and falling V, respectively. If the voltage sensitivity coefficients d_a and d_i in the more general form of Eq. (2), $k_a = k_a^0 \exp(d_a u)$ and $k_i = k_i^0 \exp(d_i u)$, were not fixed (at −0.5 and 0.5, respectively) but free as well, the information on the right hand side of the curve (e.g. the slopes in $I_{+,V=0}$ and $I_{-,V=0}$ could be used to determine these two parameters also.

Figure 3B and C shows the responses of the same system when $|dV/dt|$ of the recording protocol was increased to 1 and 10 V s^{-1}, respectively. In these cases the discontinuous changes of the capacitive currents become evident at the left and right ends of the loops. Correspondingly, the left side of the plot is split into two branches. Here the two intersections of the curves with the V-axis do not indicate, of course, the precise equilibrium voltage of the system (here E_K). The right hand side of these tracings steepens up dramatically with $|dV/dt|$ (notice different I scales in Fig. 3B and C), owing to the relatively slow and therefore incomplete reequilibration between a and i after fast and short V changes over the same amplitude.

Figure 3B$_1$ shows Fig. 3B without the capacitive up and down shifts [first term on right side of Eq. (4) ignored]. This tracing demonstrates that with a saw-tooth clamp the capacitance-corrected tracings of a V-gated conductance has the general shape of an 8, and that the

internal intersection of the 8 is located at the equilibrium voltage of the conductance. This characteristic feature is evident because the second term in Eq. (4) [with Eq. (1)] is always zero at the equilibrium voltage ($I_{GHK} = 0$), irrespective of the conductance (g_0) and the activity (p_a) of the pathway.

In general, the response to the initial sweep will differ from coinciding responses after a longer series of sweeps, i.e. the end of the initial current loop will not coincide in amount and slope with the beginning. A small discrepancy of this kind can be seen in Fig. $3B_1$. This will be the case when changes are involved which exceed the duration of a cycle. In principle, such processes could also be analyzed from coinciding responses of a longer series of consecutive sweeps. This would, however, require long recording times again, which can be avoided if only the initial cycles reflect those slower processes as well, namely by the difference in amount and change and slope of the current between the onset and the end of the cycle.

On the other hand, if the end of an individual current cycle does meet the beginning with the same slope, the response can be considered to be clean and complete, i.e. not contaminated by a drift and/or by distorting slow effects from unknown processes which partially extend into the time window under consideration.

This favorable circumstance could frequently be achieved (by selecting appropriate speed of the cycle) in the present investigations. Therefore, the theoretical examples (Figs. 1–3) have not been chosen to demonstrate the general case (individual loops not closed) rather than similarities to the clean and complete experimental recordings below.

A complete evaluation of the recorded information can be obtained by designing an adequate model for the investigated system, setting up equations like Eq. (1)–(4) and determining the involved parameters by a curve-fitting routine. This will be subject of a separate study. Here, we present a few convenient rules which allow an initial evaluation by ad hoc inspection of the records in *IV* coordinates.

1. The membrane capacitance $C_m = 0.5\Delta I/(dV/dt)$ can be read from the current jumps ΔI at the two reflection points, where dV/dt of the command voltage changes its sign. The values of both jumps have to be equal at the two reflection points.
2. It is convenient, for subsequent analysis, to subtract the capacitive currents, $\pm 0.5\Delta I$, from original tracings.
3. In capacitance-corrected tracings with one voltage-gated conductance and any non-gated conductances, an 8-shaped graph is obtained. The internal intersection occurs at the equilibrium potential of the gated transporter, whereas the current there is the current of the total, non-gated background.
4. Consider capacitance-corrected currents at a reflection point. If the amount of current of the arriving branch is smaller than that of the reflected one, the activity of the transporter is rising, and vice versa. This obvious feature discriminates outward rectifiers (more active at positive voltages) from inward rectifiers (more active at negative voltages).
5. If several voltage-gated ion pathways are involved, the (capacitance-corrected) tracings may display none or several internal intersections at positions which are not necessarily at the related equilibrium potentials but may be even outside the V range of equilibrium voltages of the pathways involved.
6. If the V position of an internal intersection does not change with $|dV/dt|$, this V position indicates an equilibrium voltage, even in the presence of several V-gated conductances.

Results and discussion

A typical cycle with $|dV/dt| = 1$ V s^{-1} over a voltage range of $\Delta V = 250$ mV (from −200 to +50 mV) lasted $2\Delta V/|dV/dt| = 0.5$ s plus the short steady state times (20 ms each) before and after the voltage changes. As already mentioned, only those "clean and complete" results are considered here, in which the current at the end of the sweep (approximately) coincided in amount and slope with the beginning of the recording. Owing to the small $|dV/dt|$ used, all the experimental tracings presented are virtually free of capacitive currents, i.e. the rules 1 and 2 do not apply here and no capacitance corrections had to be made to use the rules 3–6. Equilibrium voltages $E_K \approx -90$ mV and $E_{cl} \approx 0$ mV for electrodiffusion of K^+ and Cl^- respectively are assumed here according to Boyd and Gradmann (1999a).

Types of individual IV loops

Since *C. wailesii* changes its electrophysiological properties without obvious environmental stimuli (Boyd and Gradmann 1999a), the new method is particularly well suited to characterize individual states quickly. Figure 4 shows a variety of recordings, each representing a different electrophysiological state. An example of a quite linear recording is shown in Fig. 4A. Only closer inspection shows a slight kink around V_0 (which will be focused on below with tracing 4E), and a slight widening of the loop in the negative voltage range indicating a K^+ inward rectifier by rules 3 and 4. Compared with the other examples in Fig. 4, the tracing of Fig. 4A is displayed with the most expanded current scale; it demonstrates that with the applied $|dV/dt| = 1$ V s^{-1} in all the samples, the capacitive currents $I_C = C_m dV/dt$ can be ignored. This current would be most obvious as a discontinuous jump of $\pm 2I_C$ at the two extreme voltages where dV/dt changed its sign abruptly (see Fig. 3B and C).

The simple curvature of the current loop in Fig. 4B is reminiscent of the intrinsic outward rectification of I_{GHK}

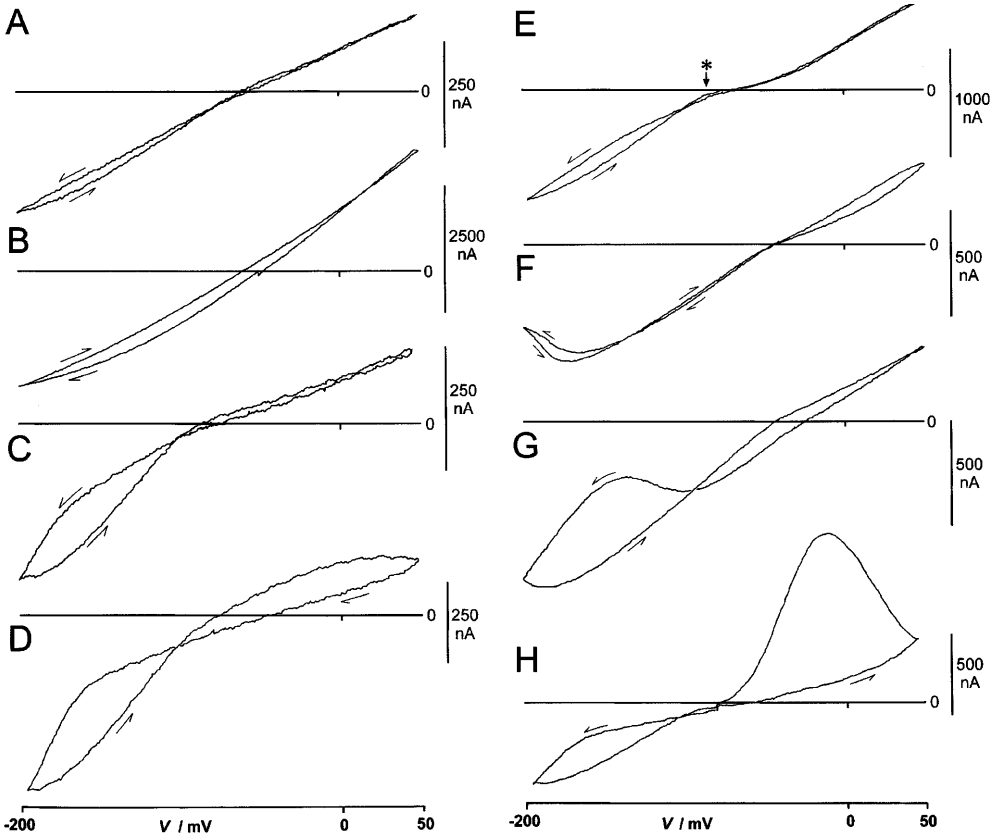

Fig. 4 Examples of different types of smoothly closed current-voltage loops of *Coscinodiscus wailesii* (with similar resting voltage), recorded by single saw-tooth voltage clamp with $dV/dt = \pm 1.0$ V s^{-1}; capacitive current steps (ca. ± 4 nA at both ends) not resolved: **A** fairly linear and coinciding branches for dV/dt positive or negative; **B** monotonic, steep positive and shallower negative branch, more curvature for negative than for positive dV/dt (lower sweep and upper sweep, respectively); **C** monotonic, inward rectifying, response to $\pm dV/dt$ essentially coinciding, shallow and linear on positive side; temporal conductance increase (wider loop) at negative voltages; **D** monotonic, 8-shaped, with temporal conductance changes (wider loop) in positive and in negative voltage range; **E** monotonic, 8-shaped, with only narrow loops in at both ends; * marks fast change in slope near E_K (≈ -90 mV), more pronounced in upward ($dV/dt > 0$) direction than in downward ($dV/dt < 0$) direction; **F** non-monotonic, parallel decrease in chord conductance (leading to negative slope conductance) at negative voltages in both (upward and downward) directions; **G** non-monotonic, strong decrease in chord conductance (leading to region with negative slope conductance) in the negative part only for $dV/dt < 0$; **H** non-monotonic, strong increase in chord conductance in positive voltage range, starting before sign change in dV/dt, peaking and terminating at $dV/dt < 0$, yielding region with negative slope after sign reversal of dV/dt

for K^+ [Eq. (1)] where the limiting slopes for outward and inward conductance correspond to $c_{K,c}$ and $c_{K,l}$, respectively. The ratio of these slopes in Fig. 4B, however, is much smaller than $c_{K,c}$:$c_{K,l} \approx 40$ in *C. wailesii* (Gradmann and Boyd 1999). One probable reason for this discrepancy is an additional 'leak' pathway (probably a Cl^- conductance) which (1) adds, on a percent basis, more to the small K^+ inward conductance than to the large K^+ outward conductance, and (2) shifts $V_{I=0}$ more positive than E_K. The negative position of the two internal intersections of the tracing 4B with the V-axis leaves no doubt about the dominant role of K^+ diffusion. According to rule 4, however, the changing conductance in Fig. 4B is not an inward rectifier, but an outward rectifier, because of the decrease in conductance between the arriving and reflected branch at the negative reflection point and the corresponding conductance increase at the positive one. In addition, the internal intersection of the tracing around 10 mV points to a V-gated Cl^- diffusion pathway. So, in Fig. 4B the relevant ion pathways are a large but time-invariant K^+ conductance and a smaller, outward-rectifying Cl^- conductance. It should be pointed out that this loop of Fig. 4B covers the largest current range of all the examples in Fig. 4. This high conductance is only partly due to the exceptionally large size of the cell (about 0.5 mm^2 compared to normal about 0.2 mm^2) from which tracing 4B was recorded. The known inward rectifying K^+ pathway in the plasmalemma of *C. wailesii* (Gradmann and Boyd 1999) is well reflected by the rising turning characteristics at negative voltages in Fig. 4C. It shows a delayed increase in K^+ conductance with negative going voltages. The left part of Fig. 4C is a typical example for the rules 3 and 4 pointing to a K^+ inward rectifier. When V has passed the negative reflection point, this K^+ conductance returns later to normal with positive going voltages but is still elevated around E_K, causing a more negative $V_{I=0}$ at this upward (positive going) branch compared with the downward (negative going) branch.

Figure 4D shows a similar behavior in the negative voltage range but also a wide loop in the positive range. The situation is closely related to that in Fig. 4C but the re-inactivation of the K^+ conductance, which was temporarily increased during hyperpolarization, was not yet completed when the command voltage returned at +50 mV. The K^+ conductance, however, returned to normal shortly after, as judged by the smooth merging of the end of the current loop with the beginning (at −80 mV). Thus the positive reflection characteristics confirm the change of an outward conductance; the *V*-position of the internal intersection of the most obviously 8-shaped tracing around −100 mV indicates that K^+ is the charge carrier of this inward rectifier.

The slender current loop in Fig. 4E consists of a "double-8", with an internal intersection at about −50 mV and another one at about −100 mV. This shape indicates that (at least) two conductances (probably for K^+ and Cl^-) with different equilibrium voltages have changed and returned completely during the sweep. In addition, Fig. 4E shows a peculiar kink, at about −85 mV (marked with an *). When the voltage moves from negative to positive, this kink consists of an approximately twofold change of the slope conductance within 5 mV; it is not as sharp as in the negative going branch of the tracing when the start and end of the loop coincide. Such kinks can be identified in several tracings of Fig. 4. As in tracing 4E, the occurrence of such a kink is frequently coupled with a double-8 shape. It is assumed that these kinks reflect steep gating of a Cl^- conductance.

Thus far, all examples here show monotonic current-voltage loops. The following three examples (Fig. 4F, G, and H), however, show portions with negative slope. In principle, the occurrence of negative slope conductances in such *IV* loops does not necessarily point to a complex gating system. This is evident from the portions with $dI/dV < 0$ in the theoretical examples in Fig. 3A, B, and D, which arise from a very simple gating system.

In Fig. 4F, negative slope conductance is evident in the far negative voltage range. In this example, this feature appears to be a steady-state property, because it is rather independent of the sign of dV/dt. Other features of this loop are known already from previous examples: widening in positive voltage range (Fig. 4D), kink, and double-8 shape (see Fig. 4E).

The portion of the current-voltage loop in Fig. 4G with negative slope conductance is also in the negative voltage range, however, without coincidence for rising and for falling voltage (as in Fig. 4F) but only for negative going voltages, after a current maximum at about −100 mV. This individual observation will be analyzed in more detail below in the context of several related *IV* loops. The (small) portion of negative slope conductance just at the beginning of the positive going branch, in Fig. 4G, may reflect the rise of g_K according to rule 4, similar but stronger as in Fig. 4C.

Finally, Fig. 4H displays a striking portion of negative slope in the positive voltage range, at the beginning of the negative going branch. According to rule 4, it is a large and temporal activity of a K^+ outward rectifier. This transient K^+ conductance starts before dV/dt changes from positive to negative. It culminates near $V = 0$ and terminates (almost) during the return of the voltage to the start voltage (here −80 mV). This individual observation will also be discussed in the next paragraph with respect to related *IV* loops.

Systematic changes of IV loops

Figure 5 shows an example of the effect of different $|dV/dt|$ on the shape of current-voltage loops. The data in Fig. 5A are the same as in Fig. 4C. It is a good example for rules 3 and 6 because all three *V* locations of the internal intersections of the 8-shaped tracings A, B, and C are near E_K. This series shows that with slower $|dV/dt|$ the inward-rectifying characteristics become more and more similar to the sigmoid steady-state K^+ transport characteristics in Fig. 5D which have been reported previously (Gradmann and Boyd 1999). The tendency to approach a time-independent saturation current in the positive range is reflected by all tracings of Fig. 5. In contrast, at negative voltage ranges the behavior is very sensitive to $|dV/dt|$. The common quali-

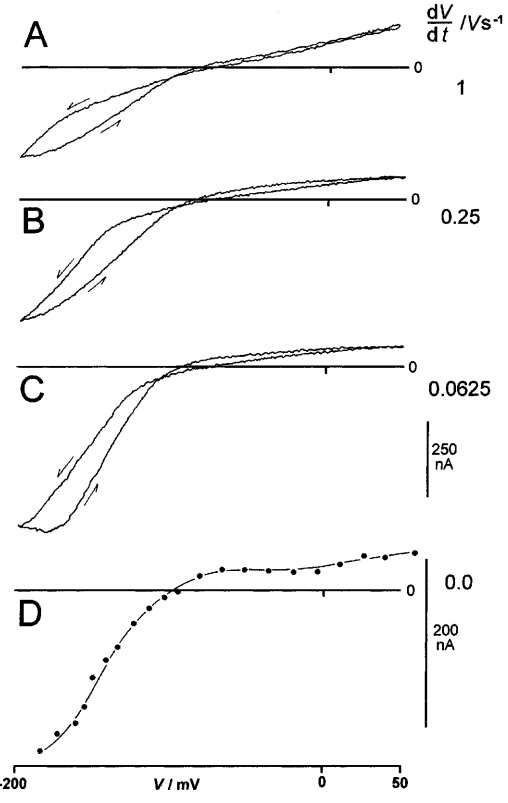

Fig. 5 Effect of different $|dV/dt|$ in single saw-tooth voltage-clamp experiments on the shape of the recorded *IV* loop: **A**, **B**, **C** data from same cell in similar states as Fig. 4C (=5A); **D** steady-state *IV* data (Gradmann and Boyd 1999) recorded from a different cell with a step protocol

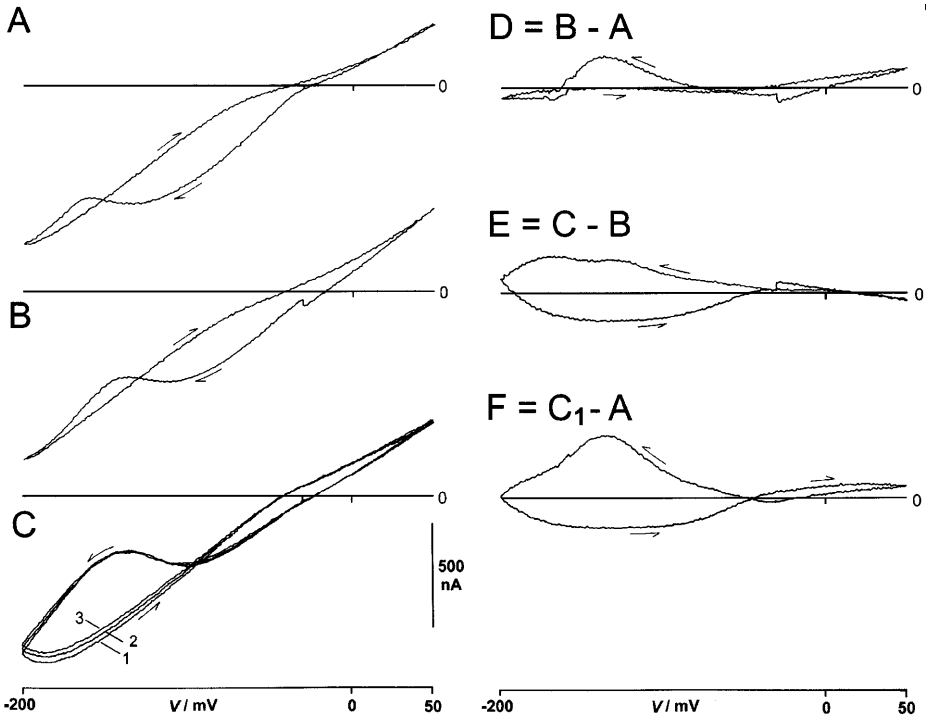

Fig. 6 Stages in development of stable state with negative slope conductance in downward branch around −150 mV upon standard saw-tooth voltage protocol. No data from stable starting state. **A** curvature in downward branch causes internal intersection with rather linear upwards branch at about −170 mV; **B** more pronounced expression of curvature in downward branch, causes shift of internal intersection to more positive voltage (about −150 mV); **C** final, stable state with three very similar recordings obtained within 1 min. **D** Difference *IV* loop (B − A) showing formation of transient outward current in downward branch; **E** difference *IV* loop (C_1 − B), showing rather horizontal downward loop (slightly tilted clockwise), and formation of transient inward current; **F** difference *IV* loop (C_1 − A) showing final change in *IV* loop with transient outward current, followed by transient inward current

tative feature is a reversible, hyperpolarization-induced increase of the K^+ conductance (rule 4). The smaller $|dV/dt|$, the more time the system spends at elevated negative voltages, and the K^+ conductance has more time to increase towards the maximum, g_0. At about −200 mV, g_0 seems to be reached nearly in Fig. 5C and completely in Fig. 5D, when the extrapolated slope ($\Delta I/\Delta V$, not illustrated) passes the origin [see Eq. (1) and discussion of Fig. 3A]. The tendency to saturate can already be seen at the end of the negative going branch in tracing B ($dV/dt = \pm 0.25$ V s^{-1}) but not in the fastest tracing A ($dV/dt = \pm 1.0$ V s^{-1}). Characteristic for a *V*-gated inward rectifier is also the finding that within the negative going branch the "critical" voltage of the conductance increase (the voltage at which the curvature of downward bending is strongest) occurs already at smaller hyperpolarizations when $|dV/dt|$ is small.

In order to analyze the processes in Fig. 4 G and H, these current-voltage loops have been subtracted[1] from current-voltage loops in the temporal vicinity which showed different degrees or even absence of negative slope conductance. The hyperpolarization-induced transient (Fig. 4G) has developed spontaneously within about 4 min from a rather linear and steady slope via the states A and B to state C_1 in Fig. 6. The three superimposed tracings (1, 2, and 3) in Fig. 6C have been recorded over another time interval of about 1 min. Their similarity demonstrates that the changes have come to a (temporal) rest in state C. The differences (tracings D, E, and F) between these tracings A, B, and C show that the whole transitions consisted of two major steps: first a development of a transient outward current [peak in the downward branch of Fig. 6D (6B − 6A)] with a relatively invariant upward branch (upward branch of difference curve 6D is close to zero). After another minute (Fig. $6C_1$ = Fig. 4G) a transient inward current has developed which follows 100–200 ms after the transient outward current under the applied voltage protocol. This development of the transient inward current is highlighted by the difference tracing of Fig. 6E ($6C_1$ − 6B), which shows in the downward branch (apart of a little clockwise tilt) a relatively constant current but a pronounced trough in the upward branch. Finally, Fig. 6F (= D + E = C_1−A) shows both transients which have developed during a few minutes.

The characteristics of state C are peculiar, especially with respect to the transient outward current around −150 mV (see Fig. 6D). Rules 3 and 4 do not apply for these tracings because there is a second internal intersection (around +20 mV, visible in tracing 6A) and, more importantly, the predominant internal intersection is not fixed at any known equilibrium voltage but moves from about −170 mV to about −110 mV between tracings 6A and 6C. Thus, rules 5 and 6 point to activity changes of (at least) two ion transporters. One might think about superimposed conductance changes of K^+ and Cl^- pathways (rule 5). On the other hand, it might

[1] There is some confusion in the literature about the "validity" of $dI(V)$ curves. Blatt (1986) has pointed out correctly that $dI(V)$ curves do not cross the *V*-axis when the parent $I(V)$ curves refer to a concentration change of a translocated ion at one side (typically outside from 0 to 1). The $dI(V)$ curves in the present study, however, do not reflect such thermodynamic differences but kinetic ones (different activities of ion transporters). Therefore, the $dI(V)$ presented here reflect $I(V)$ of the transporter of interest correctly.

also reflect the transient activity of an electrogenic pump. Previous reports (Gradmann and Boyd 1995; Boyd and Gradmann 1999a) have demonstrated, in fact, that an electrogenic pump does reside in the plasmalemma of *Coscinodiscus*, and that this pump is active only during short periods of time. So the peculiar shape of the *IV* loops in the negative voltage region of Fig. 6C might also reflect short periods of activities of the pump, caused by hyperpolarization during the applied voltage protocol.

To enable a systematic investigation of the depolarization-induced current transients (Fig. 4H), for the temporal distance of the standard voltage protocols we alternated between long (about 1 min) and short (about 6 s) times. After long pauses the characteristic, large current loops did appear in the beginning of the downward branch. Figure 7A_1 and A_2 shows the *IV* loops of two such events which have been recorded about 5 min apart (separated by additional events not illustrated). Figure 7B shows the two *IV* loops (7B_1 and 7B_2) which have been recorded only 6 s after 7A_1 and 7A_2 (=4H), respectively. In order to highlight the effect of temporal distance on the shape of the *IV* loops, the difference *IV* loops $A_1 - B_1$ and $A_2 - B_2$ are plotted in Fig. 7C as the loops C_1 and C_2, respectively. Both these difference *IV* loops show virtually zero current in the left (negative) half of the voltage range and very similar characteristics in the right half: (1) in the downward branch at about −90 mV a rather sudden onset of an inward current reminiscent of the kink pointed out in Fig. 4E; (2) at about −60 mV a peak of this inward current; (3) passage near the origin; (4) an accelerated increase of the outward conductance which continues after the voltage turn from downward to the upward branch, causing an increasing amount of the negative slope right after the sign reversal (or a point of inclination at about +25 mV in the downward branch); (5) a current maximum at about −20 mV; and (6) another inclination point around −50 mV in the downward branch before a steep return to zero difference. For purposes of illustration, the examples selected have also very similar absolute currents (e.g. the negative current peak, the current at the voltage return, and the peak of the outward current). In other examples (not shown) these amounts appeared downscaled. The global process displayed by Fig. 7C consists of a transient inward current followed by a transient outward current, both initiated by a depolarization. This pattern corresponds to electrical excitation in animals and plants.

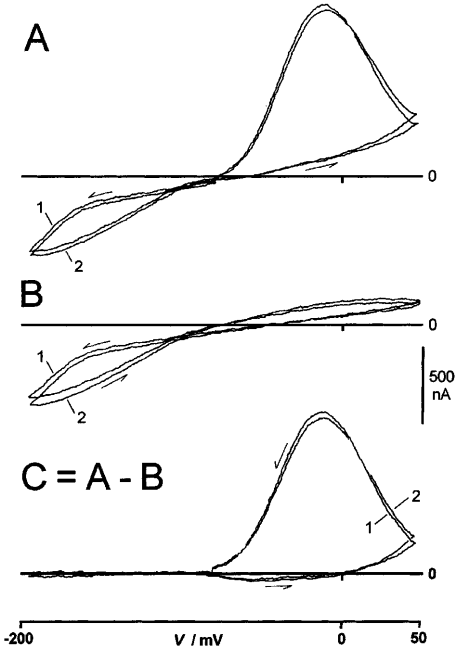

Fig. 7 Depolarization-induced excitation investigated by differences of current loops from single saw-tooth voltage protocol of excitable cell: **A** two current loops (A_1 = Fig. 4D, and A_2 recorded 5 min later) 50 s after past-induced excitation in the form of large temporal outward current in positive part of downward branch; **B** two current loops (B_1 and B_2) recorded 6 s after A_1 and A_2 respectively showing no excitation (refractory); **C** the two differences ($C_1 = A_1 - B_1$ and $C_2 = A_2 - B_2$); in left part the differences are virtually zero; in right part, temporary (smaller) inward current followed by temporary (larger) outward of both tracings equal each other in great detail

In physiological studies of animal cells it is commonly observed that tetraethylammonium (TEA^+) inhibits K^+ export (e.g. Fan and Yazulla 1997) whereas K^+ import is less affected by TEA^+ (e.g. Simasko and Sankaranarayanan 1997). In vascular plants, TEA^+ acts also with distinct kinetics on inward and on outward currents (reviewed by Thiel and Wolf 1997). Here the effect of external TEA^+ on the shape of the *IV* loops has been tested as well. The results are plotted in Fig. 8. Panel 8A shows a reference *IV* loop upon a standard voltage protocol in the absence of TEA^+. Its actual shape (double-8, probably) is complicated but not of immediate interest here. Panel 8B shows the *IV* loop of the same cell which was exposed to 10 mM TEA^+ for 1 min. The difference *IV* loop (8A − 8B) is given in panel 8C. This d*IV* loop shows a reversal voltage ($V_{I=0} = -91$ mV, averaged from the smoothened upward and downward branch) virtually coinciding with $E_K \approx -90$ mV. According to Fig. 8C, TEA^+ affects outward currents more than inward currents. One might imagine that this apparent outward rectification (of the d*IV* loop) simply reflects the different K^+ concentrations on the cytoplasmic side of the membrane (≈400 mM) and on the luminal one (10 mM) according to Eq. (1). It might, however, also reflect a larger effect of TEA^+ on K^+ export than on import as in animal cells. In order to examine this possibility, the maximum amounts of the inward and of the outward currents (at $V_1 = -200$ mV, and $V_2 = +50$ mV, respectively) have been monitored from a series of *IV* loops after exposure of the cells to 10 mM TEA^+. In Fig. 8D the results are plotted in a percentage scale versus incubation time. These data show that TEA^+ inhibits the outward currents stronger (by ca. 60%) and faster (time constant τ about 1 min) than the inward currents (by ca. 30% and $\tau \approx 3$ min, respectively). These effects are considered to be satu-

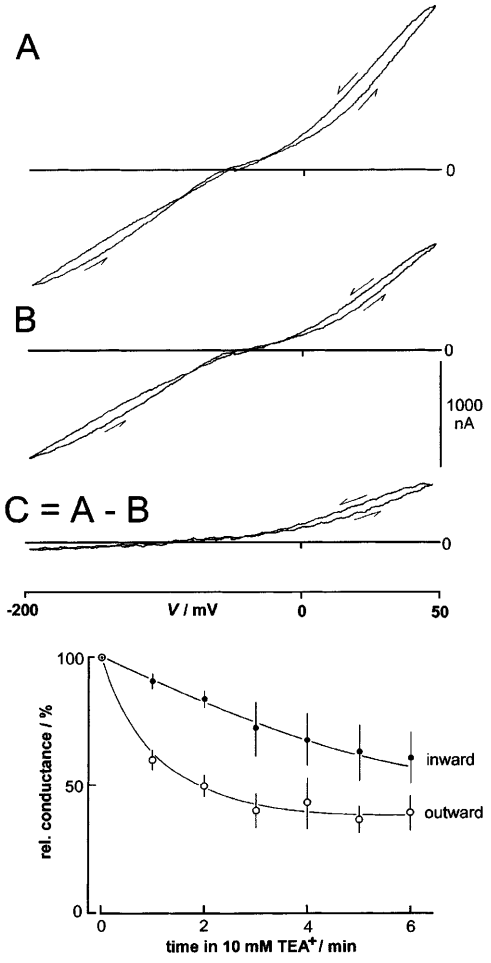

Fig. 8 Effect of TEA^+ on current loops of *C. wailesii* under voltage clamp using single saw-tooth voltage protocol with $dV/dt = \pm 1.0$ V s^{-1}: **A** control recording from one cell in the absence of TEA^+; **B** recording from the same cell, 1 min after incubation with 10 mM TEA^+; **C** difference *IV* loop **A–B**; notice reversal voltage $V_{I=0} \approx E_K \approx -90$ mV; **D** bulk data from three independent experiments on wash-in kinetics of the effects of TEA^+ on inward current and on outward current recorded at $V_1 = -200$ mV and $V_2 = 50$ mV respectively by experiments as in panels **A** and **B**; notice larger and faster effect on outward current compared to wash-in kinetics of inward current

rated, because 20 mM TEA^+ did not cause significantly larger effects. The results in Fig. 8D suggest that TEA^+ has (at least) two sites of action on K^+ conductance in *C. wailesii*, i.e. one site which is saturated earlier after exposure to 10 or 20 mM TEA^+ and causes a 60% inhibition of outward currents, plus a second site which is saturated later and causes about 40% inhibition of the inward conductance for K^+. This conclusion is confirmed immediately by interpretation of the positive reflection characteristics of tracing 8 C by rule 4, i.e. that the major effect of TEA^+ consists of the inhibition of an outward K^+ rectifier. In summary, the results in Fig. 8 suggest that many different pathways for K^+ permeation coreside in the plasmalemma of *C. wailesii*, namely not only different pathways for import and export of K^+ but also TEA^+-sensitive and TEA^+-insensitive conductances (probably channels) for inward as well as for outward currents. The residual TEA^+-insensitive currents are suggested to be carried mainly by K^+ as well, because TEA^+ caused only a depolarization by < 10 mV.

Conclusions

1. Detailed non-linear current-voltage-time relationships can be recorded in a short time by voltage-clamp experiments with single saw-tooth voltage commands.
2. Convenient rules allow an initial evaluation of the records plotted in current-voltage coordinates.
3. The cells of the marine diatom *C. wailesii* alternate between many distinct electrophysiological states, including excitation, mostly determined by voltage-gated conductances (channels) for K^+ and Cl^-.
4. TEA^+ (10 mM) partially inhibits K^+ permeation through the plasmalemma of *C. wailesii*, predominantly by inhibition of a K^+ outward rectifier.

Acknowledgements We thank Dr. Gerhard Thiel for critical reading of the manuscript. C.M.B. has been supported by grants from the Natural Sciences – Engineering Research Council of Canada.

References

Blatt MR (1986) Interpretation of steady state voltage-current curves: consequences and implications of current subtraction in transport studies. J Membr Biol 92: 91–110

Boyd CM, Gradmann D (1999a) Electrophysiology of the marine diatom *Coscinodiscus wailesii* I: endogenous changes of membrane voltage and resistance. J Exp Bot 50: 445–451

Boyd CM, Gradmann D (1999b) Electrophysiology of the marine diatom *Coscinodiscus wailesii* III: nitrogen uptake. J Exp Bot 50: 461–467

Fan SF, Yazulla S (1997) Electrogenic hyperpolarization-elicited chloride transporter current in blue cones of zebrafish retinal slices. J Neurophysiol 77: 1447–1459

Frey BW, Carl A, Publicover NG (1998) Charybdotoxin block of Ca(2+)-activated K^+ channels in colonic muscle depends on membrane potential dynamics. Am J Physiol 274: C673–C680

Gradmann D, Boyd CM (1995) Membrane voltage of marine phytoplankton, measured in the diatom *Coscinodiscus radiatus*. Mar Biol 123: 645–650

Gradmann D, Boyd CM (1999) Electrophysiology of the marine diatom *Coscinodiscus wailesii* II: potassium currents. J Exp Bot 50: 452–459

Hodgkin AL (1951) The ionic basis of electrical activity in nerve and muscle. Biol Rev 26: 339–409

Simasko SM, Sankaranarayanan S (1997) Characterization of a hyperpolarization-activated cation current in rat pituitary cells. Am J Physiol 272: E405–E414

Svirskis G, Hounsgaard J (1998) Transmitter regulation of plateau properties in turtle motoneurons. J Neurophysiol 79: 45–50

Thiel G, Wolf AH (1997) Operation of K^+-channels in stomatal movement. Trends Plant Sci 2: 339–345